CHAPTER IV
RESULTS AND DISCUSSION

The main objective of this work is to separate both oil and water from the API separator sludge. The first two parts focused on the recovery of oil from the sludge by two techniques of chemical treatment. The first technique used nonionic surfactant as a detergent to remove the oil from the solid surface and create the small oil droplets which were destabilized by electrolyte. The other technique involved the use of $FeCl_3$ and polyelectrolytes together with flotation process.

4.1 Recovery of Light Components by Using Surfactant and Electrolyte Solution

4.1.1 Composition of API Separator Sludge

API separator sludge was characterized by distillation and extraction to determine the water and solid content, respectively. Its compositions are shown in Table 4.1. Its compositions are shown in Table 4.1. It composes of 61.3, 34.64, and 4.06 wt% of water, oil and solid, respectively. The amount of oil is sufficiently high for recovery.

Table 4.1 The composition of API separator sludge

Composition	wt%
Water	61.30
Oil	34.64
Solid	4.06

4.1.2 Effect of Surfactant Type and Concentration

The recovery here is defined as the mass of the light components to that of the oil in the initial sludge as shown in Equation (4.1).

$$\%Recovery \;=\; \frac{M}{M_0}\times 100. \tag{1}$$

where M and M_0 are mass of the oil in the initial sludge and mass of the separated oil, respectively.

The results showed that the solution of surfactant in distilled water could not recover the light components from the API separator sludge. This is due to the fact that the light component droplets are stabilized by negative zeta potential which cannot be destroyed by distilled water (Stachusky *et al.*, 1996). It was then postulated that a cation of an electrolyte can reduce the magnitude of the zeta potential or decrease electrostatic repulsion between each droplet which results in coalescence of these droplets and complete oil phase separation.

Thus, in this study, the surfactant with saturated NaCl solution was introduced. As shown in Figure 4.1, the oil recovery increases as the concentration of the surfactant increases. It was found that Empilan KB-7 and Empilan NP-9 show the same trend albeit the average recovery.
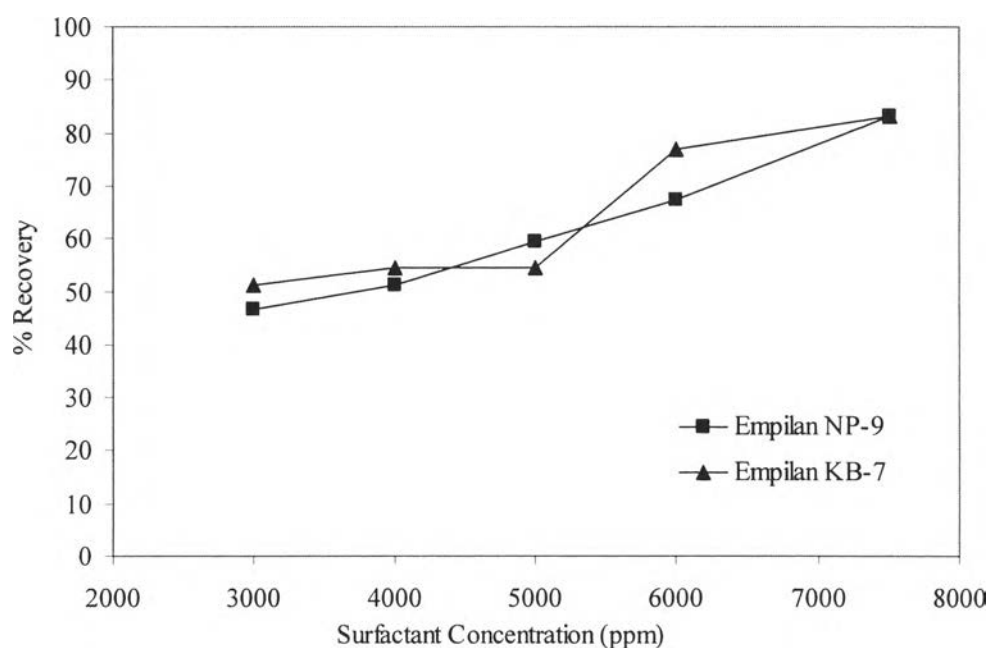
Figure 4.1 Light components recovery at various concentrations of surfactant solution.

4.1.3 Effect of Electrolyte Type and Concentration

The effect of NaCl concentration on the recovery efficiency is shown in Figure 4.2. The experiments were carried out with 5000 ppm surfactant. It was found that at the NaCl concentration less than approximately 5 wt%, the surfactant solution cannot recover the light components from the sludge. From this point, the recovery increases as the NaCl concentration increases. It should be noted that NaCl alone can also recover the light components up to 48.9%.

The role of the surfactant here is to recover the free oil in the solution and also the light components which attach to the solid surface. Further investigation also shows that the cationic charge also influences the recovery efficiency. The addition of higher charge cation has effectively induced the destabilization of the light component droplets, leading to the oil phase separation. As shown in Figure 4.3, Ca^{2+} is more efficient for the recovery of the light components than Na^+ at the same concentration. With higher positive charge of Ca^{2+}, it can reduce more electrostatic repulsion than Na^+.
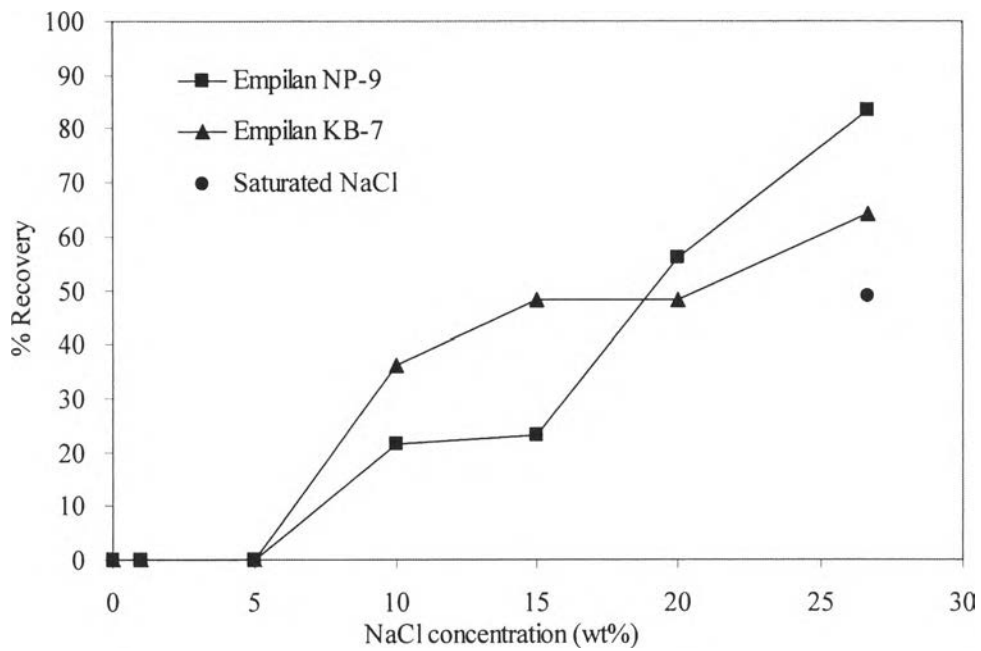
Figure 4.2   Light Components recovery at various NaCl concentrations.
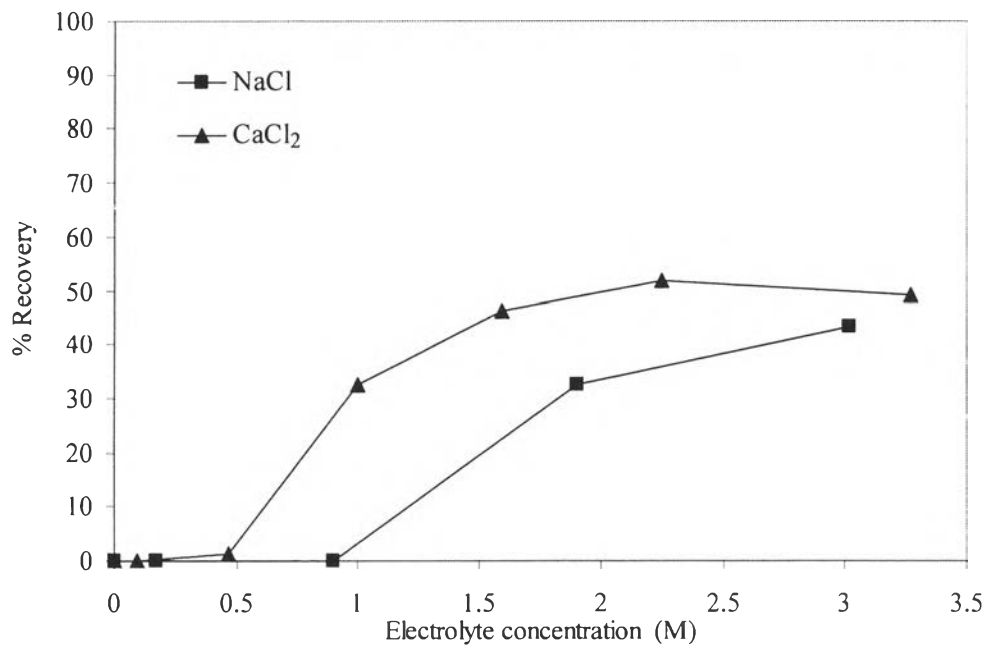
Figure 4.3   Light components recovery by using two types of electrolyte.

4.1.4   Effect of Temperature

The recovery efficiency is also affected by the operating temperature. The light component recovery by using 5000 ppm of surfactant in saturated NaCl

solution at different temperature is shown in Figure 4.4. The recovery was found to decrease as the temperature increase. This might be due to an increase in the Na^+ mobility as the temperature increases. At high mobility, Na^+ is less likely to attach to the light component droplets; as a result, negative zeta potential cannot be neutralized. That would result in the reduction in recovery efficiency.
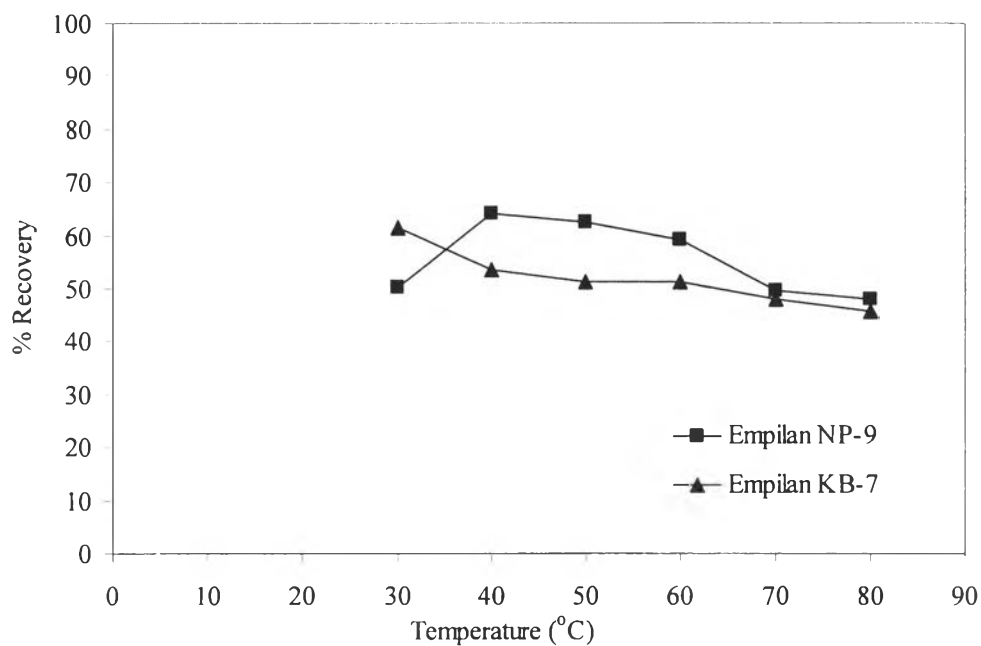
Figure 4.4 Light components recovery at various temperature.

4.1.5 Re-use of Surfactant Solution

Surfactant solution was re-used in this part to study the ability of the surfactant solution after the 1st and 2nd uses. The ratio of sludge to re-used surfactant solution remains the same for comparison purpose. The solution was measured for its total organic carbon (TOC) to determine the amount of surfactant after use. The results are shown in Table 4.2.

From Table 4.2, it was found that the amount of surfactant is reduced after the 1st and 2nd uses, respectively. Approximately 54% of surfactant are lost into the oil and solid phases after treatment process. Therefore, the concentration of surfactant solution is reduced to a half of the initial concentration which is approximately 2680 ppm. As the previous results, effect of surfactant type and

concentration, the recovery is less than 50% at that concentration. Consequently, the light components recovery decreases with the re-used surfactant solution.

Table 4.2 Total organic carbon of surfactant solution and percentage of light components recovery

Surfactant Solution	Total Organic Carbon (ppm)	% Recovery
1st use	366	64.1
After 1st use	170	46.5
After 2nd use	74	44.0

4.2 Recovery of Light Components by Using Coagulant, Flocculant and Flotation Technique

4.2.1 Effect of Coagulant Dosage and pH

$FeCl_3$ was used as a coagulant to reduce the electrostatic repulsion, leading to the agglomeration of the oil droplets. It has been demonstrated that pH and coagulant concentration are important control parameters, when coagulant chemicals are employed (Al-Shamrani *et al.*, 2002). The influence of $FeCl_3$ dosage at different pH was studied at fixed coagulant and flotation times. Figure 4.5 shows the light component recovery at different amounts of $FeCl_3$ added as a function of pH. The $FeCl_3$ dosage hardly affects the recovery for pH between 4 and 9. However, when pH is higher than 9, a drastic reduction in the recovery is observed over the range of the studied $FeCl_3$ concentration. The oil droplets have very large magnitude in negative surface potential at high pH due to the adsorption of hydroxyl ions at the oil-water interface (Marinova *et al.*, 1995). This would result in the increasing of the repulsion between oil droplets and lower the recovery. The highest light components recovery, 84.1%, is achieved at pH 9 with 50 ppm of $FeCl_3$.
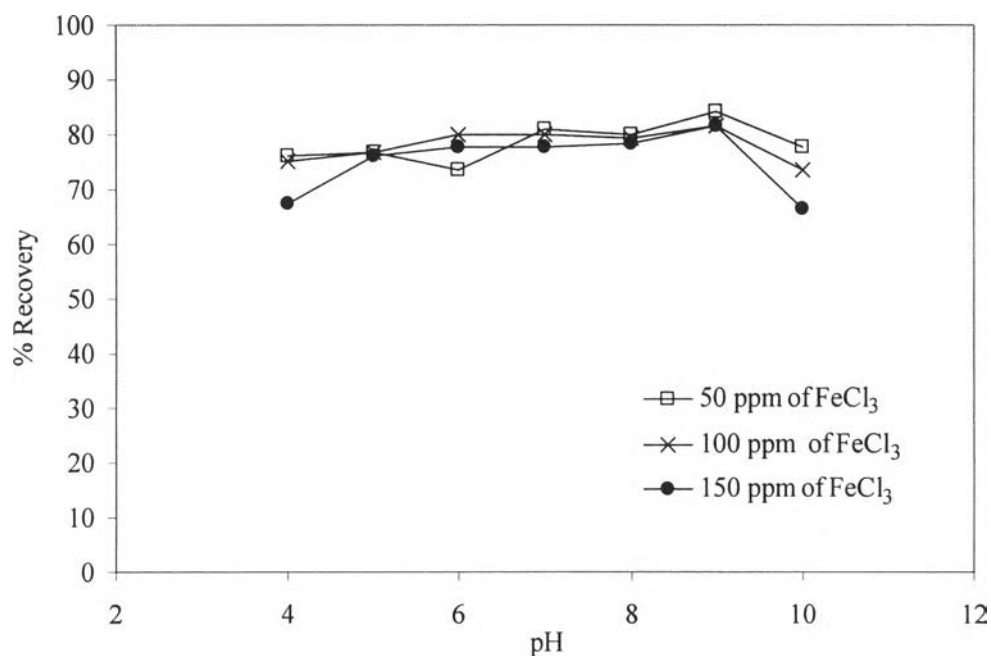
Figure 4.5 Light components recovery at different concentrations of FeCl₃ as a function of pH.

4.2.2 Effect of Surfactant on the Coagulant Performance

Empilan KB-7 was used to remove the light components from the solid surface and create the oil droplets. These oil droplets were coagulated by FeCl₃ and floated to the surface of the solution by the air bubbles. Lower light components recovery is observed for all FeCl₃ concentrations in the presence of the surfactant (Figure 4.6). This might be due to the fact that the addition of the nonionic surfactant covering the oil/water interface blocks Fe^{3+} ions to attach to the oil droplets, which results in the lower the recovery. In other words, the oil separation is hindered due to the presence of surfactant.
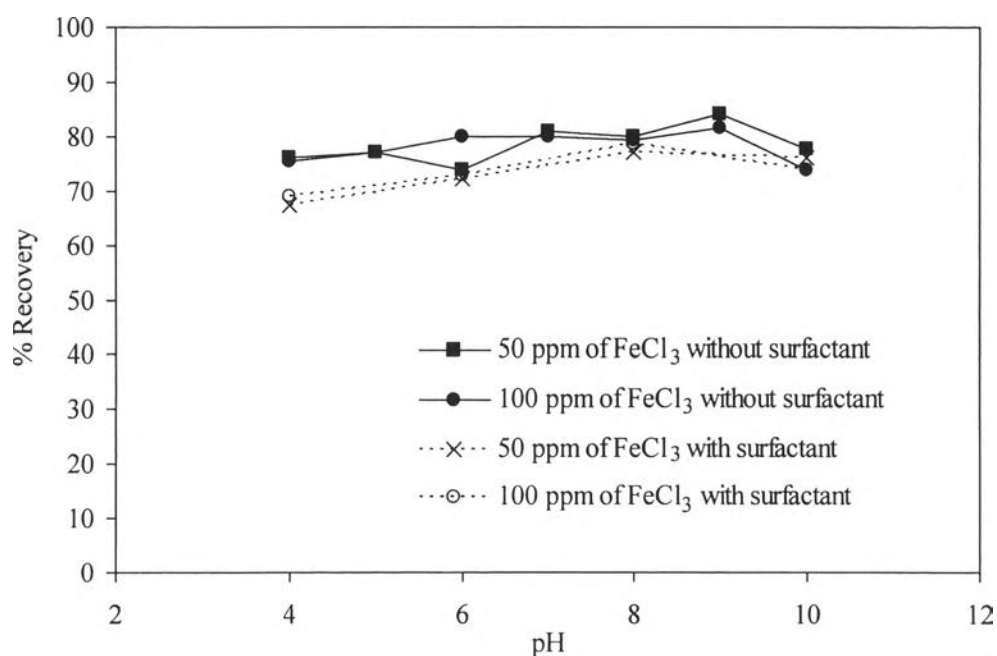
Figure 4.6 Light components recovery by using surfactant together with FeCl₃.

4.2.3 Effect of Flocculant Dosage

Addition of polyelectrolyte during oil flotation is often practiced to increase the removal efficiency. It has been proven that polyelectrolyte can enhance flotation of emulsified oil by increasing the floc size (Al-Shamrani *et al.*, 2002). Several types of polyelectrolyte which are anionic polyacrylamide with different molecular weights were used in this part. Their viscosity-average molecular weights are shown in Table 4.3. Their molecular weights were expressed in term of viscosity-average molecular weights which were calculated from their intrinsic viscosities. The recovery results by using polyelectrolyte are shown in Figure 4.7. As seen from the figure, the maximum recovery, 90-99.7%, can be obtained at very low concentration of polyelectrolyte. The optimum dosages are 5 ppm for PF2525, 10 ppm for FT2413 and FT2431, and 20 ppm for PF2628 and FT2602. However, the polyelectrolyte molecular weight has no effect on either the optimum polyelectrolyte dosage or recovery percentage. This occurs when the polyelectrolytes which their critical size cover the entire interaction area between two oil droplets are applied. From the observation of Mabire and coworkers (1984), the critical molecular weight was predicted to be 5×10^6 which is below the smallest polyelectrolyte used in this work.

Therefore, the increase in size or molecular weight of polyelectrolyte has no further effect. This is consistent with results reported by Gray and coworkers (1997).

Table 4.3 Intrinsic viscosity and viscosity-average molecular weight of polyelectrolytes

Polyelectrolyte	Intrinsic viscosity (100ml/g)	Molecular weight $\times 10^{-7}$
PF2628	150.9	5.80
FT2602	148.7	5.70
PF2525	146.0	5.57
FT2431	133.4	4.99
FT2413	129.9	4.83
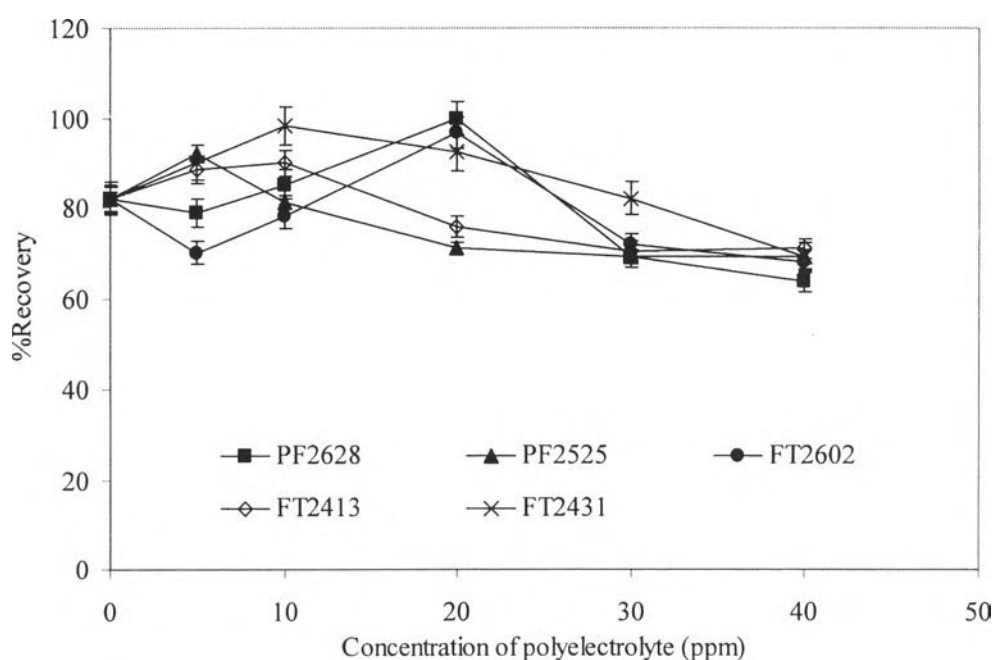
Figure 4.7 Light components recovery by using several types of polymer flocculant.

By using chemical treatment, the water was also removed which resulted in the reduction of the volume of the sludge needed to be treated by pyrolysis and the disposal cost.

4.3 Water Recovery

The treated sludge was filtrated until no more water was observed. The sludge was then distilled by using naphtha as a solvent to determine the amount of water in the treated sludge and the procedure follows ASTM D95-83. The amount of water was used to calculate the water recovery. The recovery is defined as the volume of the removed water to that of the initial water in the sludge. The results are shown in Table 4.4. Surfactant and electrolyte provide higher water recovery than the coagulant and flocculants. This may be due to the structure of flocs which contains the molecules of water such as $Fe(OH)_3$. From the comparison between oil and water recovery, polyelectrolytes provide higher oil recovery, but lower water recovery. They are more preferable for chemical treatment because less amount of chemicals are required to achieve the high recovery efficiency. On the other hand, the other systems required more concentration of surfactant and electrolyte. Also, these chemicals are expensive.

Table 4.4 Water recovery by using several chemicals to treat the API separator sludge

	%Water recovery	%Oil recovery
Empilan BK-7 and electrolyte	81.0	64.1
Empilan NP-9 and electrolyte	78.0	83.3
Ferric chloride	64.1	84.1
PF2628	67.0	99.7
FT2602	67.4	96.8
FT2413	67.0	90.0

After the API separator sludge was treated by chemical method, the residue was pyrolized at the same condition with the original sludge. This method provided the thermal decomposition data which were used to study the pyrolysis behaviors of the sludge.

4.4 Pyrolysis Behaviors of the Sludge

Pyrolysis of both original and treated sludge were operated by TGA with the heating rate of 5, 10 and 20°C/min. The thermogravimetric (TG) and derivative thermogravimetric (DTG) curves of the original sludge compared to treated sludge are shown in Figures 4.8 to 4.10. Generally, thermogram properties extracted from both curves are shifted to higher temperature when the heating rate is increased from 5 to 20°C/min. As seen from the TG curves, the original sludge provides more volatile components than the treated one does. Moreover, the TG curves shows a huge different of the final weight fraction between the original and treated sludge. The final weight fractions are approximately 44.33% and 77.31% for the original and treated sludge, respectively. This indicates that the large fraction of oil is removed during the chemical treatment process which is a convenient and cost effective method. In agreement with the previous work (Punnarattanakun *et al.*, 2002), the DTG curves clearly show that two main reaction regions exist for the original sludge pyrolysis. The first peak which represents the devolatilization of light components appears approximately between 120-400°C, while the second peak, the main pyrolysis, appears between 370-560°C depending on the heating rate. The treated sludge contains three-reaction regions: the first peak appears between 120-220°C, the second peak between 205-380°C and the last peak between 345-590°C.

From Figures 4.8 to 4.10, the disappearance of oil in the recovery process reduces the influence of the main reaction at 250-290°C as indicated by the presence of the first two peaks of the treated sludge. The last peak which represents the main pyrolysis reaction is slightly shifted to the higher temperature after the sludge was treated via the chemical treatment process. The explanation is that the remaining fractions are the heavy components which are difficult to decompose.
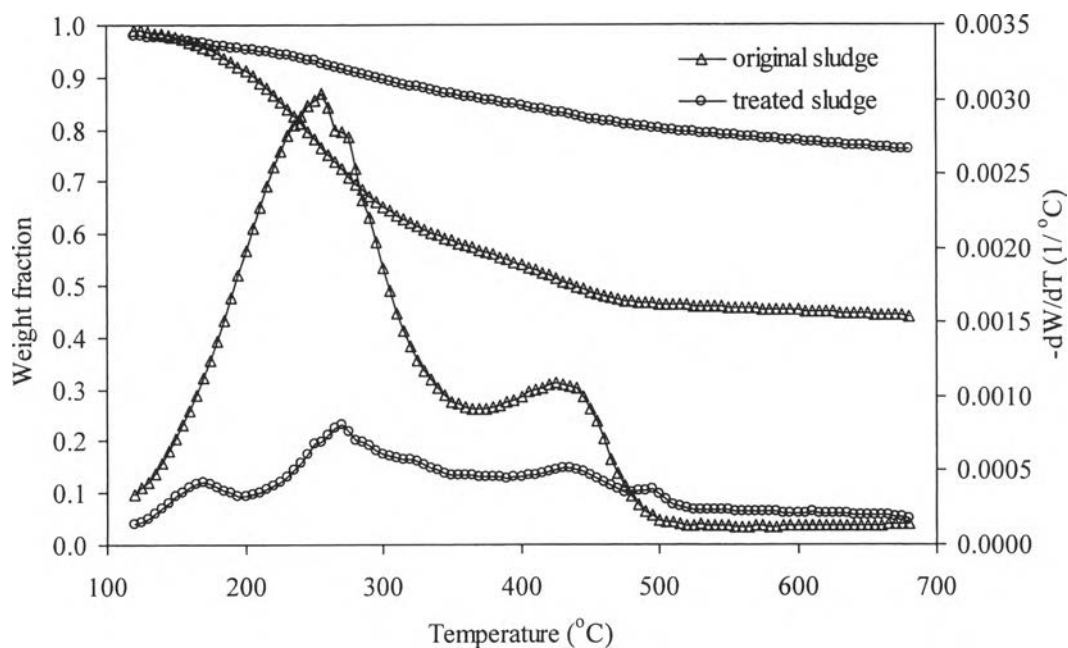
Figure 4.8 TG and DTG curves of the original and treated sludge at 5°C/min heating rate.
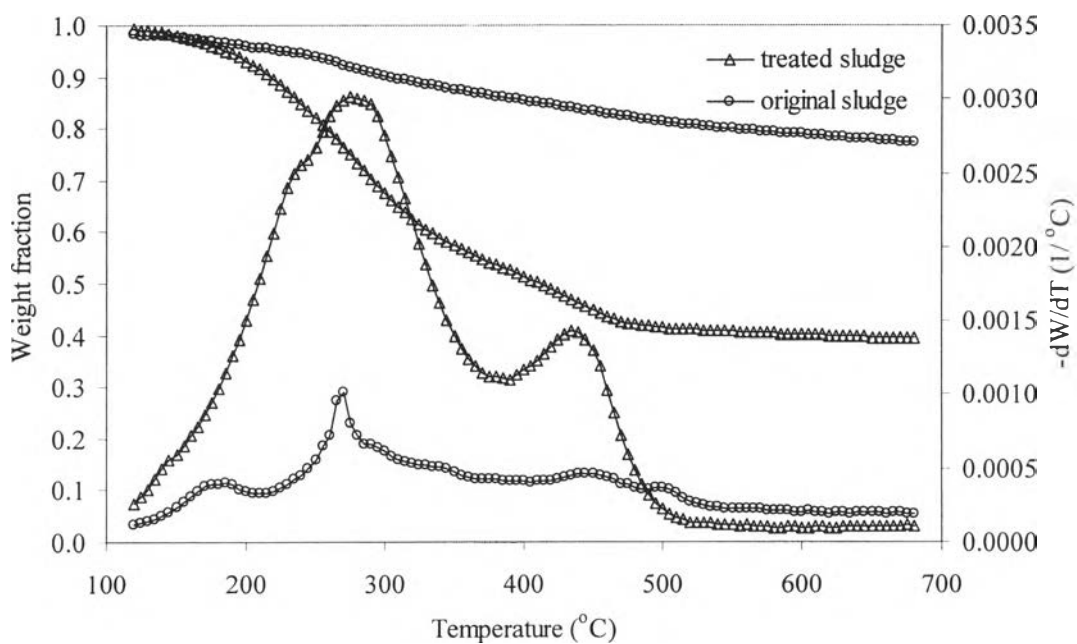
Figure 4.9 TG and DTG curves of the original and treated sludge at 10°C/min heating rate.
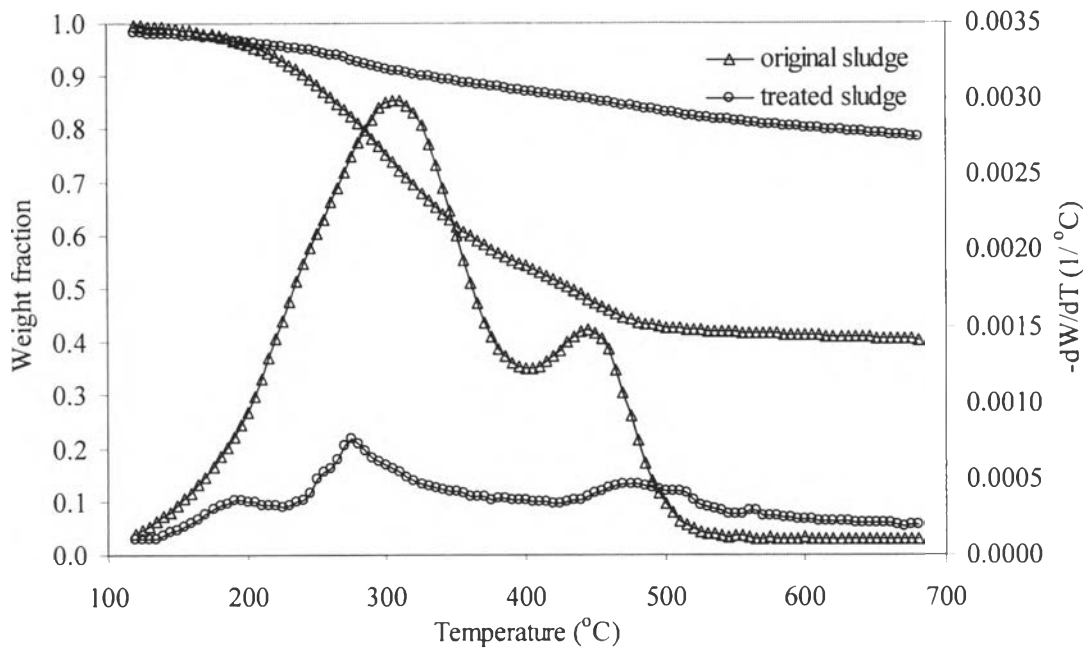
Figure 4.10 TG and DTG curves of the original and treated sludge at 20°C/min heating rate.

4.5 Mathematic Modeling

Generally, the thermal decomposition of organic material can be expressed by the equation

$$A(solid) \rightarrow B(solid) + C(gas). \tag{4.2}$$
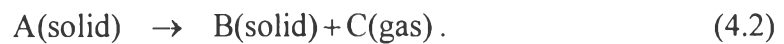
This equation is an irreversible reaction because the inert gas carries the volatile away from the pyrolysis reactor as soon as it forms. Therefore, the reverse reaction would not happen (Liu, 2002). The rate equation can be written as

$$\frac{dx}{dt} = A \exp\left(\frac{-E_a}{RT}\right) f(x), \tag{4.3}$$

where t is time used in pyrolysis and x is the weight loss fraction of reactive component. Parameters E_a and A are the activation energy and pre-exponential factor and R is ideal gas constant. The variable x can be calculated by

$$x = \frac{W - W_0}{W_\infty - W_0},$$ (4.4)

where W is the mass percentage of solid, subscripts 0 and ∞ refer to the initial and final mass percentage, respectively. When the pyrolysis is carried out with the linear temperature program, the temperature was in the form of

$$T = \beta t + T_0,$$ (4.5)

where β is the heating rate and T_0 is the initial temperature. Differentiation on both side of Equation (4.5) with respect to time gives

$$\frac{dT}{dt} = \beta.$$ (4.6)

Equation (4.2) can be written as

$$\frac{dx}{dT} = \frac{A}{\beta} \exp\left(\frac{-E_a}{RT}\right) f(x).$$ (4.7)

By rearrangement and integrating Equation (4.7), the integral equation is

$$\int_{T_0}^{T} \frac{dx}{f(x)} = \int_{T_0}^{T} \frac{A}{\beta} \exp\left(\frac{-E_a}{RT}\right) dT.$$ (4.8)

By the integral method, a function of F(x) is defined as

$$F(x) = \int_{T_0}^{T} \frac{dx}{f(x)}. \tag{4.9}$$

The right-hand side of Equation (4.8) cannot be integrated. The approximation of exponential integral term is applied to solve this equation.

$$\int_{T_0}^{T} \frac{A}{\beta} \exp\left(\frac{-E_a}{RT}\right) dT = \frac{ART^2}{\beta E_a}\left[1 - \frac{2RT}{E_a} + \ldots\right] \exp\left(\frac{-E_a}{RT}\right). \tag{4.10}$$

Coupling Equations (4.8), (4.9) and (4.10), hence

$$F(x) = \frac{ART^2}{\beta E_a}\left[1 - \frac{2RT}{E_a} + \ldots\right] \exp\left(\frac{-E_a}{RT}\right). \tag{4.11}$$

The independent pseudo bi-component model is applied for the weight loss of the sludge.

$$\frac{dx}{dT} = \begin{cases} \dfrac{dx_1}{dT} & W_{10} < W < W_{1\infty} \\[2mm] \dfrac{dx_2}{dT} & W_{1\infty} = W_{20} < W < W_{2\infty} \end{cases}, \tag{4.12}$$

where

$$\frac{dx_1}{dT} = \frac{A_1}{\beta} \exp\left(\frac{-E_{a1}}{RT}\right) f_1(x_1), \tag{4.13}$$

$$\frac{dx_2}{dT} = \frac{A_2}{\beta} \exp\left(\frac{-E_{a2}}{RT}\right) f_2(x_2). \tag{4.14}$$

For a reaction that satisfies $f(x) = (1 - x)^n$, where n is the order of the reaction

$$F(x) = \begin{cases} -\ln(1-x) & n = 1 \\ \dfrac{1-(1-x)^{1-n}}{1-n} & n \neq 1 \end{cases} \tag{4.15}$$

The TGA data are used to calculate the DTG data. Then, DTG curve is divided into two temperature intervals. By using the approximation proposed by Coats and Redfern (1964), Equation (4.11) can be written as

$$\ln\left(\frac{F(x)}{T^2}\right) = \ln\frac{A_i R}{\beta E_{ai}}\left(1 - \frac{2RT}{E_{ai}}\right) - \frac{E_{ai}}{RT}. \tag{4.16}$$

Generally, the term $\dfrac{2RT}{E_{ai}}$ is much less than unity for the thermal decomposition of polymer material. A plot of $\ln\left(\dfrac{F(x)}{T^2}\right)$ against $\dfrac{1}{T}$ should result in a straight line of the slope $\dfrac{-E_{ai}}{R}$ and the y-intercept $\ln\dfrac{A_i R}{\beta E_{ai}}\left(1 - \dfrac{2RT}{E_{ai}}\right)$ for the correct reaction. This is a method to find the suitable function of f(x) of global pyrolysis kinetic. Activation energy and pre-exponential factor of each section can be calculated from the slope and y-intercept, respectively. For finding the refined A_i, Equation (4.16) is arranged to

$$\ln\left(\frac{F(x)}{T^2}\right) = \ln(S) - \frac{E_{ai}}{RT}, \tag{4.17}$$

where

$$S = \frac{A_{iR}}{\beta E_{ai}}\left(1 - \frac{2RT}{E_{ai}}\right). \tag{4.18}$$

With this equation, A_i can be calculated at any temperature. Then, the values of A_i at various temperature are plotted to express the relationship between A_i and T. Refined A_i can be obtained from

$$A_i = \frac{\int_{T_0}^{T} Ai(T)dT}{dT}.$$

(4.19)

In order to obtain the refined E_{ai}, Equation (4.16) is applied. It is rearranged by moving all variable from the right-hand side to the left-hand side. The new function is defined as $f(E_{ai})$

$$f(E_{ai}) = \ln\left(\frac{F(x)}{T^2}\right) - \ln\frac{A_i R}{\beta E_{ai}}\left(1 - \frac{2RT}{E_{ai}}\right) + \frac{E_{ai}}{RT} = 0.$$

(4.20)

Numerical method is used to solve this equation. All kinetic parameters are substituted into Equation (4.8) to test the model. For the nth order reaction which is not equal to 1, the weight fractions are calculated by

$$x = 1 - \left[1 - (1 - n)\frac{A_i RT^2}{\beta E_{ai}}\exp\left(\frac{-E_{ai}}{RT}\right)\left(1 - \frac{2RT}{E_{ai}}\right)\right]^{\frac{1}{1-n}}.$$

(4.21)

After the model is fitted to the experimental data, the mean relative error of the fitting is calculated by

$$\overline{\varepsilon_r}(\%) = \sqrt{\frac{\sum_{i=1}^{N}\left(\frac{W_{i,exp} - W_{i,cal}}{W_{i,exp}}\right)^2}{N}} \times 100,$$

(4.22)

where N is the number of the experimental data used in the fitting.

From these equations, the kinetic parameters and the mean relative errors can be calculated. They are shown in Table 4.5. For the original sludge, it is obvious

that the reaction orders of both reactions are different. On the other hand, the reaction orders of the treated sludge are approximately the same. The activation energy of the treated sludge pyrolysis is less than that of the original sludge at the same temperature range for all heating rate. As for the first reaction region is concerned, the activation energies of the original sludge are slightly lower than those of biomass, activated sludge and PVC and PET polymers observed by Liu *et al.* (2002), Chu *et al.* (2000) and Dubdub and Tiong (2001), respectively. They are approximately 62-100, 78-85 and 142-178 kJ/mol for biomass, activated sludge and PVC and PET polymers, respectively. As for the second reaction region, the activation energies of all materials show the values in the same range from approximately 100-240 kJ/mol. Nevertheless, the activation energies of treated sludge are much lower than those of hydrocarbon materials in both reaction regions. From the table, the mean relative errors are less than 1.5% for all cases. The curve fitting are shown in the Figures 4.11-4.13. These figures indicate that the kinetic models of pseudo bi-component provide a good fit to the experimental data of the original and treated sludge, respectively.
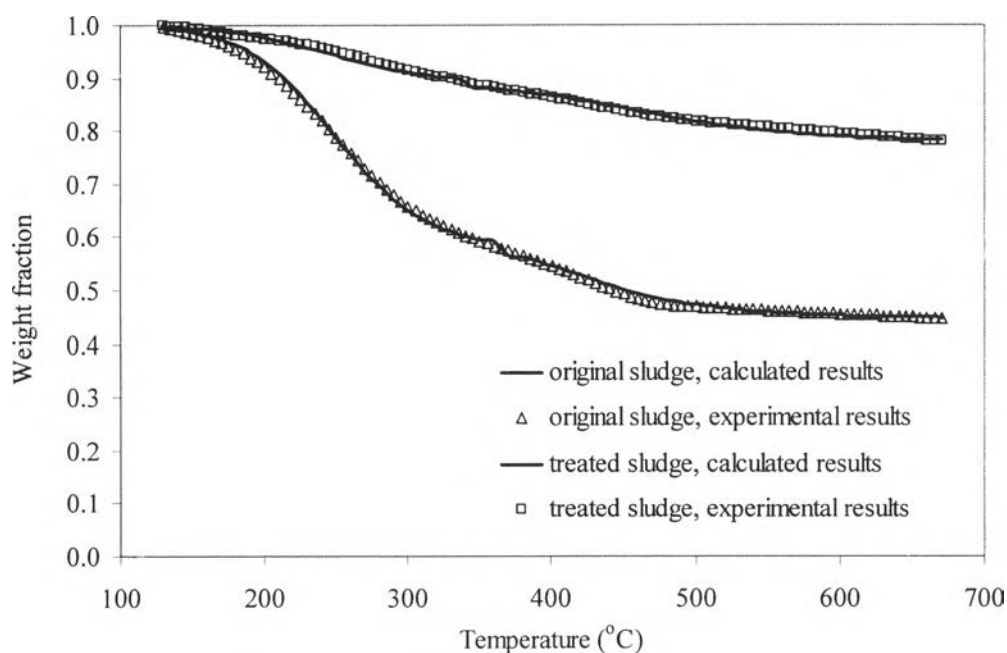
Figure 4.11 Comparison of TG curves of the experimental and calculated results at 5°C/min heating rate.
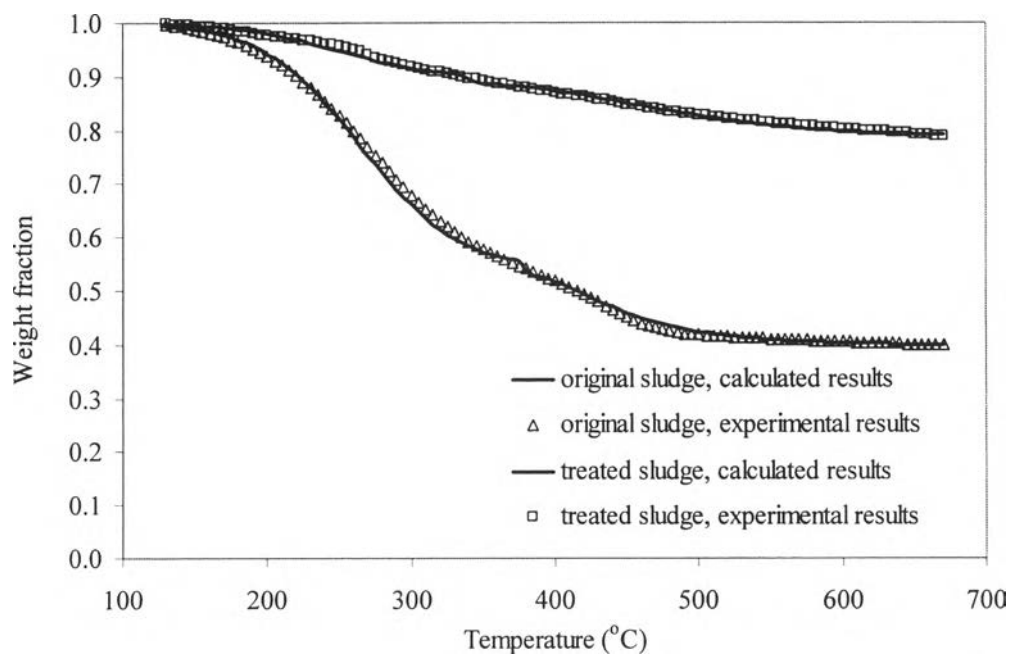
Figure 4.12 Comparison of TG curves of the experimental and calculated results at 10°C/min heating rate.
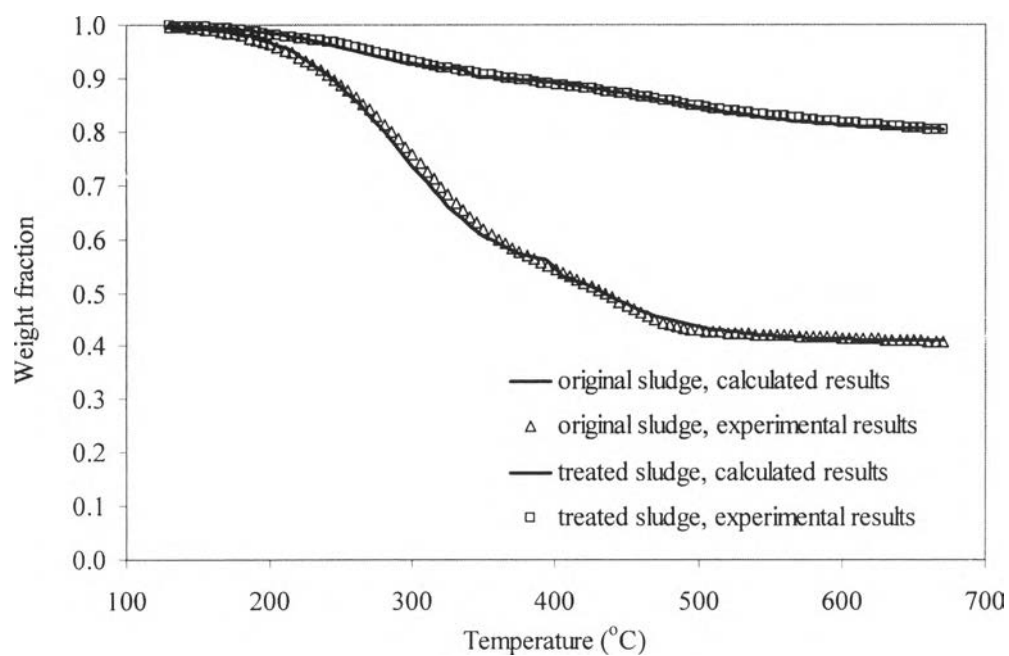
Figure 4.13 Comparison of TG curves of the experimental and calculated results at 20°C/min heating rate.

Table 4.5 Kinetic parameters of the model and the mean relative errors for the original and treated sludge pyrolysis

Type of sludge	Heating rate (°C/min)	Reaction step	Reaction order	E_{ai} (kJ/mol)	ln (A) (min^{-1})	Mean relative Error (%)
Original sludge	5	1	1.6	55.58	14.69	0.92
		2	3.0	138.25	26.11	
	10	1	1.4	50.15	12.90	1.27
		2	3.6	203.39	37.62	
	20	1	1.3	50.36	12.40	1.26
		2	3.8	239.67	43.29	
Treated sludge	5	1	1.4	44.55	11.95	0.50
		2	1.8	66.09	12.29	
	10	1	1.4	46.74	12.45	0.40
		2	1.7	63.34	11.70	
	20	1	1.3	47.49	12.53	0.38
		2	1.5	60.72	11.02	